AD-A130 296 EFFECTS OF INTERSTAGE DIFFUSER FLOW DISTORTION ON THE PERFORMANCE OF A 15..(U) NATIONAL AERONAUTICS AND SPACE ADMINISTRATION CLEVELAND OH LE.. K L MCLALLIN ET AL. 1/1

UNCLASSIFIED 1983 NASA-E-1621 NASA-TM-83359 F/G 20/4 NL

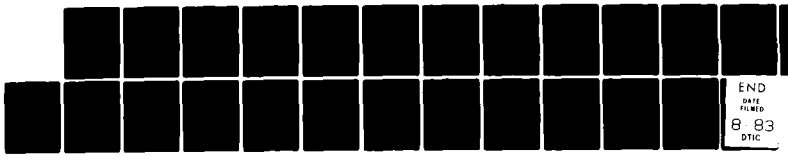

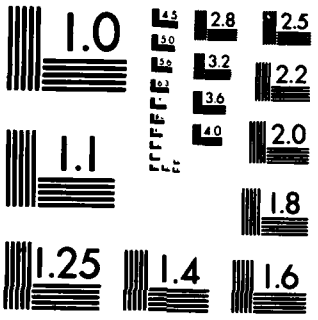

DOE/NASA/51040-46
NASA TM-83359
AVRADCOM TR-83-C-2
AIAA-83-1179

Effects of Interstage Diffuser Flow Distortion on the Performance of a 15.41-Centimeter Tip Diameter Axial Power Turbine

Kerry L. McLallin and Milton G. Kofskey
National Aeronautics and Space Administration
Lewis Research Center

and

Kestutis C. Civinskas
Propulsion Laboratory
AVRADCOM Research and Technology Laboratories
Lewis Research Center

Work performed for
U.S. DEPARTMENT OF ENERGY
Conservation and Renewable Energy
Office of Vehicle and Engine R&D

Prepared for
Nineteenth Joint Propulsion Conference
cosponsored by the AIAA, SAE, and ASME
Seattle, Washington, June 27-29, 1983

DISCLAIMER

Printed in the United States of America

Available from
National Technical Information Service
U.S. Department of Commerce
5285 Port Royal Road
Springfield, VA 22161

NTIS price codes[1]
Printed copy: A02
Microfiche copy: A01

[1]Codes are used for pricing all publications. The code is determined by the number of pages in the publication. Information pertaining to the pricing codes can be found in the current issues of the following publications, which are generally available in most libraries: *Energy Research Abstracts (ERA); Government Reports Announcements* and Index (*GRA* and I); *Scientific and Technical Abstract Reports (STAR);* and publication, NTIS-PR-360 available from NTIS at the above address.

DOE/NASA/51040-46
NASA TM-83359
AVRADCOM-TR-83-C-2
AIAA-83-1179

Effects of Interstage Diffuser Flow Distortion on the Performance of a 15.41-Centimeter Tip Diameter Axial Power Turbine

Kerry L. McLallin and Milton G. Kofskey
National Aeronautics and Space Administration
Lewis Research Center
Cleveland, Ohio 44135

and

Kestutis C. Civinskas
Propulsion Laboratory
AVRADCOM Research and Technology Laboratories
Lewis Research Center
Cleveland, Ohio 44135

Work performed for
U.S. DEPARTMENT OF ENERGY
Conservation and Renewable Energy
Office of Vehicle and Engine R&D
Washington, D.C. 20545
Under Interagency Agreement DE-AI01-77CS51040

Prepared for
Nineteenth Joint Propulsion Conference
cosponsored by the AIAA, SAE, and ASME
Seattle, Washington, June 27-29, 1983

EFFECTS OF INTERSTAGE DIFFUSER FLOW DISTORTION ON THE PERFORMANCE OF A 15.41-CENTIMETER TIP DIAMETER AXIAL POWER TURBINE

Kerry L. McLallin and Milton G. Kofskey

National Aeronautics and Space Administration
Lewis Research Center
Cleveland, Ohio 44135

and

Kestutis C. Civinskas

Propulsion Laboratory
AVRADCOM Research and Technology Laboratories
Lewis Research Center
Cleveland, Ohio 44135

Abstract

The performance of a variable-area stator, axial flow power turbine was determined in a cold-air component research rig for two inlet duct configurations. The two ducts were an interstage diffuser duct and an accelerated-flow inlet duct which produced stator inlet boundary layer flow blockages of 11 percent and 3 percent, respectively. Turbine blade total efficiency at design point was measured to be 5.3 percent greater with the accelerated-flow inlet duct installed due to the reduction in inlet blockage. Blade component measurements show that of this performance improvement, 35 percent occurred in the stator and 65 percent occurred in the rotor. Analysis of inlet duct internal flow using an Axisymmetric Diffuser Duct Code (ADD Code) were in substantial agreement with the test data.

Introduction

An axial-flow power turbine stage for application in the Chrysler/DOE Automotive Gas Turbine Engine[1-4] has been evaluated experimentally to determine the effects of interstage diffuser exit flow distortion on power turbine performance. Two inlet ducts were tested with the power turbine blading, one was the interstage transition diffuser and the other was a modified accelerating-flow duct which provided a uniform flow at stator inlet. The experimentally and analytically determined internal flow conditions in the ducts are compared. The turbine blading experimental performance with the two inlet ducts is compared in terms of blade row loss and stage efficiency.

The power turbine stage was evaluated experimentally in a component research rig[5]. The interstage diffuser duct (IDD) was included in these stage tests to determine its effect on power turbine performance. The measured turbine blading total efficiency was about 0.10 less than the design value of 0.85. The interstage diffuser was found to induce a large radial distortion of the flow at stator inlet caused by flow separation in the duct. This inlet flow distortion should adversely affect turbine performance. To evaluate the effect of this inlet distortion on turbine blading performance, an accelerating-flow duct (AFD) was designed to provide radially uniform flow conditions at stator inlet. Using a computer code for viscous, turbulent, compressible swirling flow in axisymmetric ducts (ADD Code)[6,7,8], the shroud wall contour was modified to produce uniform flow conditions at stator inlet.

This paper presents the experimentally determined performance of the power turbine stage and blading components. Turbine performance parameters are compared for distorted and uniform inlet flow conditions. The experimental data were obtained with the component research rig operated at nominal inlet conditions of 320 K and 0.408 atmospheres. These inlet conditions allow design point operation in the research rig at design Reynolds number. Turbine stage performance is presented in terms of total efficiency at three stator throat areas. The experimentally and analytically determined internal flow characteristics of the interstage diffuser duct and the accelerated-flow duct are presented in terms of radial variations in total pressure and flow angle at stator inlet. Blading component losses are also presented.

Symbols

A	annulus area
B	blocked-area fraction
c	blade chord
C_r	specific heat at constant pressure
D	blade surface diffusion parameter
h	passage height
Δh	turbine work
i	blade incidence
L	blade aerodynamic loss
n	incidence loss exponent
N	turbine rotation speed
P	pressure
r	radius from turbine centerline
R	gas constant
R_t	turbine flow Reynolds number
R_x	blading reaction based on relative velocities
s	blade spacing
T	temperature
U	blade speed
V	absolute velocity
W	relative velocity
w	mass flow rate
α	absolute flow angle
γ	ratio of specific heats
τ	turbine torque
η	turbine efficiency
λ	work factor, $\Delta h/U_m^2$
ρ	density

Subscripts

1	inlet plenum

2	preswirl vane exit
3	duct exit/stator inlet
4	stator exit/rotor inlet
5	rotor exit
cr	critical velocity
D	design
e	effective
EQ	equivalent conditions
i	incidence
in	inlet
m	mean
max	maximum
o	blade throat
x	axial component

Superscripts

-	mass average
'	total state condition

Research Facility

Apparatus

The subject turbine includes the interstage diffuser duct (IDD), power turbine stator vanes and rotor, and the exit diffuser of the DOE/Chrysler Upgraded Automotive Gas Turbine Engine[1]. The free shaft power turbine is an axial-flow design[4] with pivoting stator vanes to vary stator throat area for engine control and braking. The design point is aerodynamically conservative with a work factor of 1.247 and an equivalent total pressure ratio of 1.712 (see Table I). The blade turning angles are relatively low and velocity levels are subsonic. The variable stator can rotate between concentric spherical endwalls which keep vane end clearances constant at 1.8 percent of passage height (see Table II). The mechanical constraints imposed by the stator actuation gearing result in a design with 23 vanes having a relatively long chord (low aspect ratio) to satisfy aerodynamic loading criteria (see Table II). Likewise mechanical constraints imposed by the casting process result in an integrally cast rotor with 53 blades. With optimum solidity this constraint results in a design aspect ratio of 1.29 for the rotor (see Table II). The design tip clearance was 3 percent of passage height and this clearance was set for the subject cold-air performance tests. The turbine design, having stator end clearances, large rotor tip clearance, and limited blade numbers (low aspect ratio), is then limited also in the efficiency level it can achieve. The design estimate of total efficiency for this turbine was 0.85.

The turbine research package (see fig. 1) includes the interstage diffuser duct between the compressor-drive turbine and the power turbine. Preswirl vanes are used at interstage diffuser inlet to provide the design compressor-drive turbine exit swirl angle, approximately 20 degrees. The three support struts, the stator vanes, and the rotor are engine hardware.

The support hardware for the research turbine includes an airbrake dynamometer to absorb and measure the power output of the turbine and an inlet and exhaust piping system with flow controls (see fig. 2). Pressurized dry air was piped into the turbine through a filter, an electrical heater, a calibrated flat-plate orifice (mass flow rate measurement), and a remotely controlled pressure regulating valve. The air passed through the turbine and was exhausted through a system of piping and a remotely controlled valve into the laboratory low-pressure exhaust system. The airbrake dynamometer was cradle-mounted on air bearings for reaction torque measurement using a commercial strain-gage load cell. The rotational speed was measured with a magnetic pickup and a shaft-mounted gear.

Instrumentation

The turbine performance parameters were determined by measurement of internal temperatures, pressures, and flow angles and by the speed, torque, and mass flow rate measurements discussed in the section Apparatus. The research turbine flow path, measurement stations, and instrumentation are shown in figure 3. The instrumentation setup was the same for both the IDD and AFD inlets. The turbine efficiency was based on measurements taken at stations 3 and 5. Stator component performance was based on measurements taken at stations 3 and 4 along with paddlewheel fluid torque measurements (see fig. 4).

Turbine inlet total temperature was measured at station 1 (see fig. 3b). Inlet duct wall static pressures were measured at one circumferential position (see fig. 3a). Turbine inlet total pressure was based on the radial surveys of total pressure, total temperature, and flow angle taken at three circumferential positions at station 3 (see fig. 3a and b) which is about 1/2 a stator chord upstream of the stator leading edge. At stator exit (station 4), wall static pressures were measured (see fig. 3b). For stator component performance the turbine rotor was replaced with a paddlewheel rotor for fluid torque measurement using the bearing package and the airbrake load cell to transmit and measure the torque (see fig. 4). Turbine exit total pressures were measured by three radial survey probes at station 5 (see fig. 3b). Wall static pressures were also measured.

Procedure

Stage Performance. Data were taken at nominal stator inlet total state conditions of 320 K and 0.409 atmospheres. These inlet conditions allow operation at design Reynolds number in the research rig. Data were obtained over a range of stator-inlet-total to rotor-exit-static pressure ratios from 1.16 to 3.50, over a range of speeds from 0 to 130 percent of design, and over a range of stator throat area from 79.3 to 117.6 percent of design (stator vane-chord setting angle range from 30 to 40 degrees).

Friction torque of the bearings, seals, coupling windage, and rotor disk windage was obtained by measuring the amount of torque required to rotate the shaft and rotor disk over the range of speeds encountered in this investigation. The turbine cavity was evacuated to a pressure of 3.21 N/cm^2 which is approximately the pressure level in the rotor disk cavity during stage tests. Based on nominal test inlet conditions, the friction torque at design speed was 0.21 N-m which was about 18 percent of the turbine aerodynamic torque at design point. Friction torque was added to the dynamometer torque to obtain the turbine aerodynamic torque.

The turbine total efficiency was based on pressure measurements taken at stations 3 and 5 as well as the measurements of temperature, speed, torque, and mass flow rate (see equation 1).

$$\eta'_{3-5} = \frac{Nr}{w} \Big/ \left\{ C_p T'_3 \left[1 - \left(\frac{P'_5}{P'_3} \right)^{\frac{\gamma-1}{\gamma}} \right] \right\} \quad (1)$$

The turbine inlet (station 3) total pressure, P'_3, was determined from a correlation of mass-averaged total pressure as a function of mass flow rate, w, and inlet static pressure, P_3, based on turbine inlet radial surveys (see section Instrumentation). This was done to account for the large radial gradients in total pressure and flow angle at the turbine stator inlet with the interstage diffuser duct. The overall total pressure at rotor exit, station 5, was calculated from mass flow rate, static pressure, total temperature, and flow angle with the following equation:

$$P'_5 = P_5 \left[\frac{1}{2} + \frac{1}{2} \right.$$

$$\left. \times \left(1 + \frac{2(\gamma - 1)R}{\gamma} \left(\frac{w\sqrt{T'_5}}{P_5 A_5 \cos \alpha_5} \right)^2 \right)^{1/2} \right]^{\frac{\gamma}{\gamma - 1}} \qquad (2)$$

Stator Performance. Data were taken at nominal stator inlet total state conditions of 295 K and 0.409 atmospheres. Data were obtained over a range of stator-exit-static to stator-inlet-total pressure ratios from 0.380 to 0.921 and over a range of stator throat area from 79.3 to 117.6 percent of design.

Stator performance was determined from measurements of pressure, temperature, torque, mass flow rate, and calculations based on conservation of mass and tangential momentum at stator exit. The stator inlet total pressure was determined from the same correlation of turbine inlet total pressure as that discussed in the section Stage Performance. Stator exit fluid torque was measured with the paddlewheel rotor configuration shown in figure 4 and described in the section Instrumentation. An air barrier was used to equalize the pressures between the stator exit shroud and the shroud-paddlewheel rotor clearance gap to prevent flow leakage around the paddlewheel rotor.

Results and Discussion

Turbine Inlet Ducts

The interstage diffuser duct (IDD) (see fig. 5) was designed[4] to provide efficient diffusion of the flow during the transition from the smaller diameter gas generator turbine to the larger diameter power turbine in the DOE/Chrysler Automotive Gas Turbine Engine. The overall diffuser geometry was defined within geometry constraints to inlet and exit annulus areas and duct length based on the Sovran and Klomp correlations[9]. The length-to-inlet-height ratio is 4.5 and the area ratio from preswirl vane exit to stator exit (station 3) is 1.9. The wall contours were developed using the MERIDL code[10], an axisymmetric inviscid analysis, to provide a smooth increase in wall static pressures. There are 3 support struts in the duct with a total flow blockage of 2 percent.

The IDD inlet provides a distorted flow field into the power turbine stage which is significantly off of design[5]. To determine the effect this distortion had on turbine performance, the inlet duct shroud wall and preswirl vanes were redesigned to produce "near design" stator inlet velocity diagrams (see figure 5). The shroud wall diameter upstream of the stator was increased such that the annulus area decreased from preswirl vane exit to stator inlet providing an accelerating flow field in the duct. The shroud wall contour and the new preswirl vanes were designed using a recently available analysis code, the Axisymmetric Diffuser Duct Code (ADD)[6], for turbulent, swirling, compressible flow in axisymmetric ducts. The duct length-to-inlet height ratio was 2.2 and the exit-to-inlet annulus area ratio was 0.83.

Experimental and analytical variations in wall static pressures were determined for both ducts between preswirl vane exit and stator inlet (0 to 100 percent of duct axial length). The ADD Code analyses are based on measured duct inlet flow conditions with initial wall boundary layer displacement thicknesses of about 2.5 percent of passage height. The comparison of data with the ADD Code analysis for the IDD inlet is shown in figure 6a near design mass flow rate. Wall static pressures are normalized by duct inlet total pressure. Wall static pressures increase smoothly to stator inlet. The ADD Code analysis predicts wall static pressures very well up to 55 percent of duct length where a large hub wall flow separation is predicted. The ADD Code cannot handle large flow separation so the solution was terminated. The location of separation on the hub wall is along the compression ramp in the strut region (see fig. 5).

The comparison of data with the ADD Code analysis for the accelerated-flow duct (AFD) is shown in figure 6b. The wall static pressures are again smooth but decrease slightly near stator inlet as the flow accelerates through the area reduction. The ADD Code solution predicts gradient trends and pressure levels which are similar to the data.

The radial variations of flow angle, stator incidence, and total pressure at stator inlet are shown in figure 7 for the IDD inlet at three turbine mass flow rates. For the two lower mass flow rates, figures 7a and b, the variation of flow angle is significantly different than design at passage heights greater than 60 percent. The total pressure is distorted to a greater extent in this region, although distortion exists over the entire span. For the high mass flow rate, the flow angle distortion is still limited to passage heights greater than 60 percent but the gradient is larger. The total pressure variation is greatly distorted over the entire passage height. As mentioned above, the ADD Code analyses indicated flow separation at 55 percent of duct length. Stable solutions could not be generated at the stator inlet plane.

The radial variations of flow angle, stator incidence, and total pressure at stator inlet are shown in figure 8 for the AFD inlet near design equivalent mass flow rate. Both data and the ADD Code solution are shown. The design stator inlet angle is about 31 degrees. The AFD inlet provides a relatively uniform distribution of measured flow angle. The stator incidence, at design setting (see fig. 8a), is near optimum incidence over the entire passage height with a variation from -8 degrees at 20 percent to -3 degrees at 95 percent of passage height. The radial variation in measured total pressure is relatively uniform (see fig. 8b), although a small deficit in total pressure exists

from 30 percent of passage height to the hub. The ADD Code results are also shown in figure 8. While in general trends in radial variations are predicted, the level of flow angle is about 3 degrees off over most of the passage. Also, the total pressure deficit in the hub region was predicted to be similar to that measured although magnitudes are different. Preswirl vane geometries are modelled by the ADD Code as a body force applied to the flow based on airfoil section loss correlations. This model is not detailed enough to predict all preswirl vane loss phenomena and may result in the discrepancies between data and analysis noted above. The radial variations for the AFD inlet are shown only at design flow since these variations were similar at all mass flow rates tested.

The survey data, as shown in figures 7 and 8, can be used to calculate the effective annulus area, A_e, necessary to pass the volume flow rate if the passage velocity were uniform at the maximum measured value. A blocked-area fraction, B, can then be computed from the effective and actual annulus areas.
This blocked-area fraction would be an indication of the nonuniformity of flow across the passage. Larger B values indicate greater flow nonuniformity. Based on Sovran and Klomp[9], the effective area is calculated as:

$$A_e = 2\pi \int_{r_n}^{r_t} V/V_{max}\ r\ dr \qquad (3)$$

where the local velocity, V, and the maximum velocity, V_{max}, are calculated from the survey data. The blocked-area fraction is:

$$B = 1 - A_e/A \qquad (4)$$

Blocked-area fractions were calculated for the surveys taken at stator inlet for both inlet ducts. The surveys were conducted over a wide range of mass flow rates. The blocked-area fractions are shown as a function of equivalent mass flow rate for both inlet ducts over the range of mass flow rates tested (see fig. 9). The trends in blockage shown are markedly different for the two inlet ducts. The AFD inlet blockage is constant over the range of mass flow rates with a value of about 0.03. However, the IDD inlet blockage varies over a wide range with a minimum value of 0.11 near design mass flow rate, and blockage increases sharply for mass flow rates greater than 0.65 Kg/s. The IDD inlet has almost 4 times the stator inlet blockage of the AFD inlet at design mass flow rate.

Turbine Component Performance

Turbine stator and rotor component losses for IDD and AFD inlets are compared at design speed and work for 3 stator throat areas (79.3, 100, and 117.6 percent of design). The average stator inlet conditions for these comparison points are shown in Table III in terms of blockage (B_3), flow angle (α_3), incidence (i_3), critical velocity ratio (V_3/V_{cr}), and equivalent mass flow rate (w_{eq}). For the closed stator throat area case the stator settings for IDD inlet and AFD inlet were not the same so that a direct comparison at this condition is not possible (see Table III). As stator throat area increases turbine mass flow rate also increases. For the IDD inlet this means increasing flow blockage and flow distortion. Additional effects include large stator incidence and inlet velocities at 117.6 percent throat area. The AFD inlet conditions remain uniform with lower blockage and inlet velocities. The increase in stator incidence shown in the table for the AFD inlet is due to the pivoting of the vane chord as the stator is opened to larger throat areas since the inlet flow angle (α_3) is constant.

The stator component losses, in terms of efficiency points, are compared in figure 10a for the IDD and AFD inlets. At design throat area the stator loss is 1.4 points less with the AFD inlet. Performance is also improved at the other throat areas with a trend of increasing improvement with increased throat area. The two factors influencing these trends are the differences in inlet blockage and the large stator incidence produced with the IDD inlet at the larger throat areas.

The rotor component losses in terms of efficiency points are compared in figure 10b for the IDD and AFD inlets. At design throat area the rotor loss is 2.6 points less with the AFD inlet. The difference in rotor loss between IDD and AFD inlets is nearly the same at all three stator throat areas. Rotor losses increase with increasing stator throat area. Rotor inlet conditions cannot be defined from hub to tip due to lack of detailed measurements, but on a mass averaged basis the majority of the rotor loss increase with throat area increase is probably due to incidence losses.

The turbine stage total efficiencies are compared in figure 10c for the IDD and AFD inlets. At design stator throat area, the turbine total efficiency difference is 4 points (5.3 percent) due to the large reduction in turbine inlet flow blockage and distortion provided by the AFD inlet. Of this 4-point improvement, 35 percent is due to reduced stator losses while 65 percent is due to reduced rotor losses. It is apparent that a major impact of inlet flow distortion on turbine efficiency is in the rotor. The difference in turbine efficiency for the two inlet ducts increased linearly with stator throat area with differences of 3, 4, and 5 points for throat areas of 79.3, 100, and 117.6 percent, respectively.

Stator and rotor incidence losses were estimated based on the mass averaged flow conditions. The loss model used[11] assumes that the velocity component normal to the blade inlet mean camber line is lost kinetic energy.

$$L_i = \frac{\bar{W}_{in}^2}{2}\left(1 - \cos^n(\bar{i})\right) \qquad (5)$$

In equation 5 the exponent, n, is 2 for negative incidence and 3 for positive incidence. The difference in component incidence losses between the IDD and AFD inlets are shown in figure 10d in terms of efficiency points. The difference in stator incidence loss increases from 0.5 to 6.0 points as the throat area increases from 79.3 to 117.6 percent of design due to the increasingly distorted flow conditions of the IDD inlet (see Table III). The difference in rotor incidence loss between IDD and AFD inlets is near zero. These incidence losses are based on mass averaged values of W_{in} and i and do not reflect the effects of the radial variation of these values on a true mass averaged incidence loss. In general, for these turbine configurations, incidence loss is a significant factor in stator losses

due to inlet flow distortion but incidence effects were not obvious from the data for rotor losses due to inlet flow distortion.

Turbine Exit Radial Surveys

Rotor exit radial surveys of total pressure, total temperature, and flow angle were taken at design speed, design stator throat area, and a total pressure ratio (P_3'/P_5') of 1.74 with the IDD inlet and the AFD inlet. Radial variations in flow angle (α_5), total temperature drop ($1-T_5'/T_3'$), and total efficiency (η_{3-5}') are shown in figure 11. The flow angle distribution from hub to tip (see fig. 11a) is similar for the two inlet ducts with a sudden increase in flow angle in the tip region from 75 to 95 percent of passage height due to blade unloading in the tip clearance gap (test clearance of 3 percent). The absolute level of flow angle, however, is less (more negative) with the AFD inlet indicating greater rotor flow turning at the same ideal total enthalpy. The largest differences in flow angle occur, not in the tip region where the inlet distortion is greatest, but from 5 to 50 percent of passage height. This effect is more apparent in figure 11b which shows the radial variation in total temperature drop through the turbine (an indication of the radial work distribution). The turbine inlet temperature was radially constant for both inlet ducts. While the outer half of the blade span has nearly the same temperature drop, the inner half has a much higher temperature drop with the AFD inlet. Since the ideal total enthalpy is the same for both surveys, this difference in temperature is reflected in higher total efficiency in this section of the blade span for the AFD inlet (see fig. 11c). The local total efficiency is between 5 and 10 points higher for the AFD inlet between 5 and 50 percent of passage height. A high loss region exists for both inlet ducts in the tip region due to the relatively large tip clearance used.

A comparison of the inlet and exit radial distributions of normalized mass flux for the IDD and AFD inlet ducts is shown in figure 12. The inlet radial distributions of mass flux are shown for radial surveys near design mass flow rate (see fig. 12a) for both inlet ducts. The local mass flux has been normalized by the mass averaged value for each duct such that uniform free vortex flow with no boundary layers would have a constant normalized mass flux of 1.0. As expected from the survey results shown in figures 7 and 8, the IDD inlet has a large deficit in mass flow in the tip region. The normalized mass flux decreases sharply from the peak value of 1.2 at 55 percent of passage height to 0.37 at 95 percent. The mass flux distribution for the AFD inlet is relatively uniform from hub to tip with a peak value of only 1.04 at 70 percent of passage height.

The rotor exit radial distributions of mass flow for the IDD and AFD inlet ducts are shown in figure 12b. The survey data presented in figure 11 were used. The equivalent mass flow rates for these surveys are 0.630 kg/s and 0.652 kg/s for the IDD and AFD inlets, respectively. As seen in figure 9 the blockage parameter, B, for the IDD inlet is relatively constant in this flow range so the comparison of these inlet and exit mass flow distributions is valid. The radial distributions of normalized mass flux are similar for both inlet ducts with greater than average exit flow at mid-span where peak efficiencies occur and in the tip clearance gap region. While the inlet mass flux distributions are markedly different for the two inlet ducts (see fig. 12a) the flow is redistributed in passing through the blading so that the inlet radial distortion in flow is not apparent at rotor exit.

Summary

An axial-flow power turbine stage has been evaluated experimentally to determine the effects of interstage diffuser flow distortion on turbine performance. The turbine blading was tested with the interstage transition diffuser duct (IDD) and a modified accelerated-flow duct (AFD) which provided uniform flow at stator inlet. The experimentally and analytically determined internal flow conditions in the ducts are compared. Turbine blading experimental performance with the two inlet ducts is compared in terms of blade row loss and stage efficiency. Rotor exit radial surveys of total pressure, total temperature, and flow angle are compared for the two inlet ducts in terms of absolute flow angle, total temperature drop, total efficiency, and normalized mass flux.

The two inlet duct configurations produced markedly different radial distributions of stator inlet flow conditions. The stator inlet flow blockages were measured to be 11 percent and 3 percent for the IDD inlet and the AFD inlet, respectively. While the AFD inlet provided radially uniform flow conditions into the stator the IDD inlet produced large radial gradients in flow angle, total pressure, and mass flux from 60 percent of passage height to the tip. Comparison of analytical results (Axisymmetric Diffuser Duct Code (ADD)) to the measured data indicated good agreement on wall static pressures and agreement in radial total pressure distribution trends at stator inlet for the AFD. Simplified preswirl vane loss models may be limiting ADD Code agreement with data.

Turbine stage total efficiency at design speed and work was 5.3 percent greater with the uniform inlet conditions of the AFD inlet as opposed to the distorted inlet flow of the IDD inlet. Blading component measurements indicate that, of this performance improvement, 35 percent occurred in the stator and 65 percent occurred in the rotor. Stator inlet and rotor exit radial surveys indicate that the stage efficiency increase with improved inlet conditions is due to better blading performance from hub to mid-span. The highly distorted radial distribution of mass flow of the IDD inlet is redistributed through the turbine stage as rotor exit radial variations in mass flow are similar for both IDD and AFD inlets.

The results presented herein graphically demonstrate the extreme adverse impact interspool/interstage transition duct induced flow distortion can have on small axial turbine stage efficiency. Turbine efficiency losses resulting from stage inlet flow distortion were presented in terms of an inlet blockage correlation parameter. The subject research program identifies the need for detailed studies of both transition duct internal flows and turbine blading performance with distorted inlet flows. The ADD Code was shown to be a useful tool for analysis of viscous flows in small turbine ducts although improvements are needed. In the future, both fundamental turbine research and sophisticated viscous flow analyses methods will be necessary to improve turbine performance in the small gas turbine environment.

References

1. Ball, G. A., Gumaer, J. I., and Sebestyen, T. M., "The ERDA/Chrysler Upgraded Gas Turbine Engine—Objectives and Design," SAE Paper 760279, 1976.
2. Galvas, M. R., "Compressor Design for the Energy Research and Development Agency (ERDA) Automotive Gas Turbine Program," NASA TM X-71719, 1975.
3. Roelke, R. J., and McLallin, K. L., "The Aerodynamic Design of a Compressor-Drive Turbine for Use in a 75-Kilowatt Automotive Engine," NASA TM X-71717, 1975.
4. Kofskey, M. G., Katsanis, T., and Schumann, L. F., "Aerodynamic Design of a Free Power Turbine for a 75-Kilowatt Gas Turbine Automotive Engine," NASA TM X-71714, 1975.
5. McLallin, K. L., Kofskey, M. G., and Wong, R. Y., "Cold-Air Performance of a 15.41-Centimeter Tip Diameter, Axial Flow, Power Turbine With Variable-Area Stator Designed for a 75-Kilowatt Automotive Gas Turbine Engine," NASA TM-82644, 1982.
6. Anderson, O. L., "Finite-Difference Solution for Turbulent Swirling Compressible Flow in Axisymmetric Ducts with Struts," NASA CR-2365, 1974.
7. Anderson, O. L., Hankins, G. B., and Edwards, D. E," "Extension to an Analysis of Turbulent Swirling Compressible Flow for Application to Axisymmetric Small Gas Turbine Ducts," United Technologies Research Center, East Hartford, Conn., R81-915395-12, Dec. 1981. (NASA CR-165597).
8. Anderson, O. L., Hankins, G. B., and Edwards, D. E., "Users Manual for Axisymmetric Diffuser Duct (ADD) Code, Vols. I, II, and II," United Technologies Research Center, East Hartford, Conn., UTRC81-65, Dec. 1981. (NASA CR-165598).
9. Sovran, G., and Klomp, E. D., "Experimentally Determined Optimum Geometries for Rectinlinear Diffusers with Rectangular, Conical, or Annular Cross-Section," Fluid Mechanics of Internal Flow, edited by G. Sovran, Elsevier Publishing Co., New York, 1967, pp. 270-312.
10. Katsanis, T., and McNally, W. D., "Revised Fortran Program for Calculating Velocities and Streamlines on the Hub-Shroud Midchannel Stream Surface of an Axial-, Radial-, or Mixed-Flow Turbomachine or Annular Duct," NASA TN D-8430, 1977.
11. Glassman, A. J., Turbine Design and Application, Vol. III, NASA SP-290, 1972.

TABLE I. - DESIGN POINT FOR THREE OPERATING CONDITIONS

Parameter	Hot condition	Equivalent condition	Test condition
Inlet total temperature, T_3',K	1154	288.2	319.4
Inlet total pressure, P_3', N/cm^2	19.55	10.13	4.137
Mass flow rate, kg/s	0.590	0.624	0.242
Specific work, J/g	137.1	35.1	38.9
Turbine rotative speed, rpm	46 150	23 343	24 577
Torque, N-m	16.74	8.96	3.66
Rotor blade speed, U_m, m/s	331.4	167.6	176.5
Work factor,λ	1.247	1.247	1.247
Total pressure ratio, P_3'/P_5'	1.678	1.712	1.712
Static pressure ratio, P_3'/P_5	1.827	1.867	1.867
Overall static pressure ratio, P_3'/P_6	1.738	1.776	1.776
Total efficiency, η_{3-5}'	0.850	0.850	0.850
Static efficiency, η_{3-5}	0.741	0.741	0.741
Overall static efficiency, η_{3-6}	0.800	0.800	0.80
Gross power (road load, 104 km/hr),[a] kW	30.1	11.3	4.9
Gross power (design),[a] kW	80.9	21.9	9.41
Turbine Reynolds number, R_t	1.90×10^5	5.05×10^5	1.83×10^5

[a]Design speed.

TABLE II. - BLADING GEOMETRIC AND AERODYNAMIC DESIGN PARAMETERS

Parameter	Stator			Rotor		
	Hub	Mean	Tip	Hub	Mean	Tip
Chord, c, cm	1.900	2.151	2.403	1.463	1.311	1.278
Leading-edge radius, cm	0.076	0.089	0.102	0.048	0.038	0.028
Trailing-edge radius, cm	0.025	0.030	0.036	0.030	0.025	0.018
Solidity, c/s	1.16	1.15	1.14	2.053	1.613	1.399
Aspect ratios, h/c	-----	0.789	-----	-----	1.29	-----
Reaction,[a] R_x	0.883	0.857	0.845	0.505	0.771	0.823
Diffusion,[a] D	0.399	0.395	0.377	0.461	0.482	0.325
Clearance, cm	0.015	-----	0.015	-----	------	0.051
(percent of h)	(0.9)	-----	(0.9)	-----	------	(3.0)

[a]Stator aerodynamic parameters for design setting angle of 35.3.

TABLE III. - AVERAGE STATOR INLET CONDITIONS AT DESIGN VALUES OF SPEED AND WORK

Duct	$A_T/A_{T,D}$, percent	B_3, percent	α_3, deg	i_3, deg	$(V/Vcr)_3$	W_{eq}, Kg/s
IDD	79.3	12.2	37.9	-10.6	.298	.548
	100.0	11.1	43.5	-21.5	.386	.636
	117.6	15.0	48.6	-31.3	.485	.702
AFD	75.3	3.0	28.3	-1.0	.256	.530
	100.0	3.0	28.4	-6.4	.321	.655
	117.6	3.0	28.3	-11.0	.359	.724

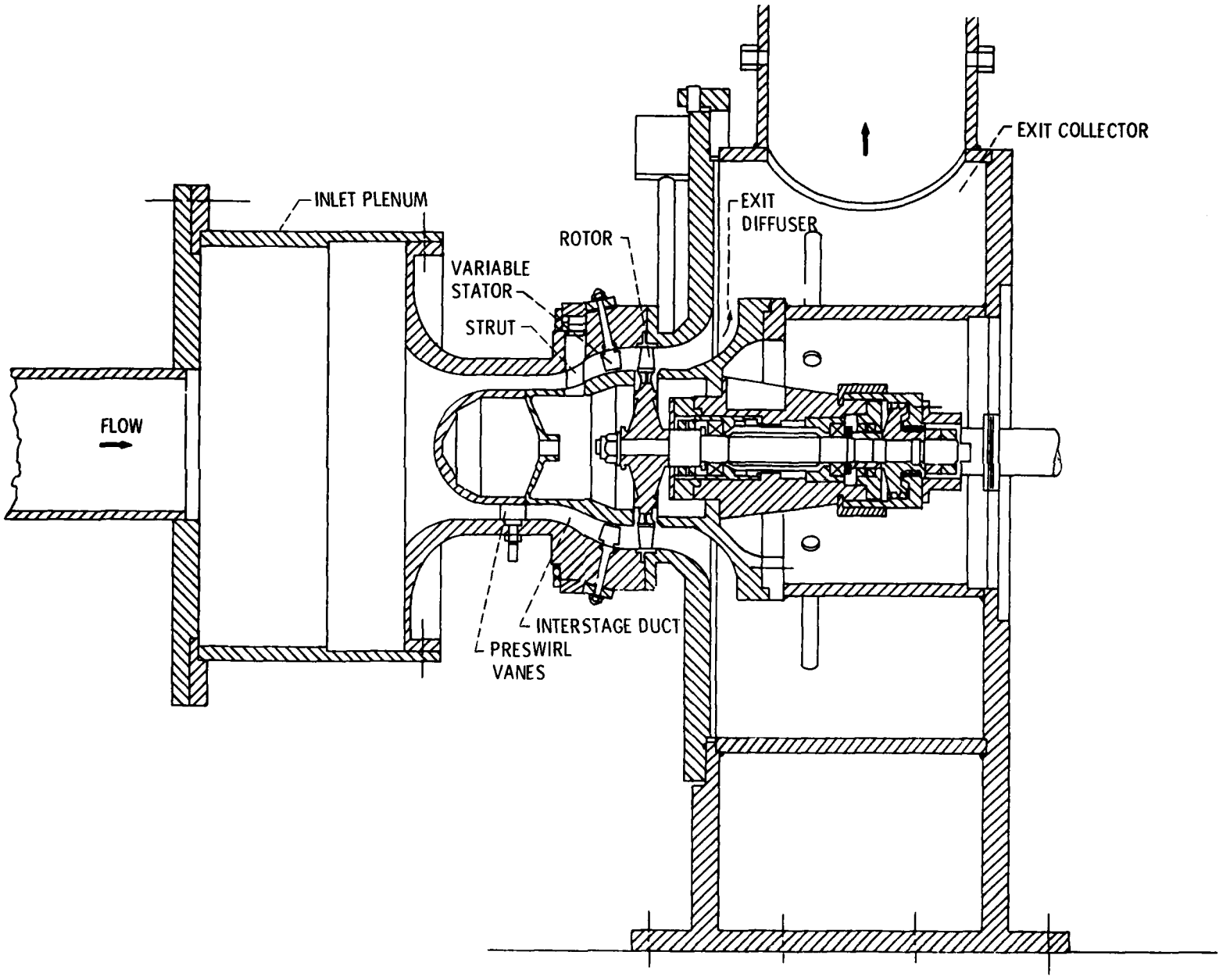

Figure 1. - Schematic of turbine used for tests.

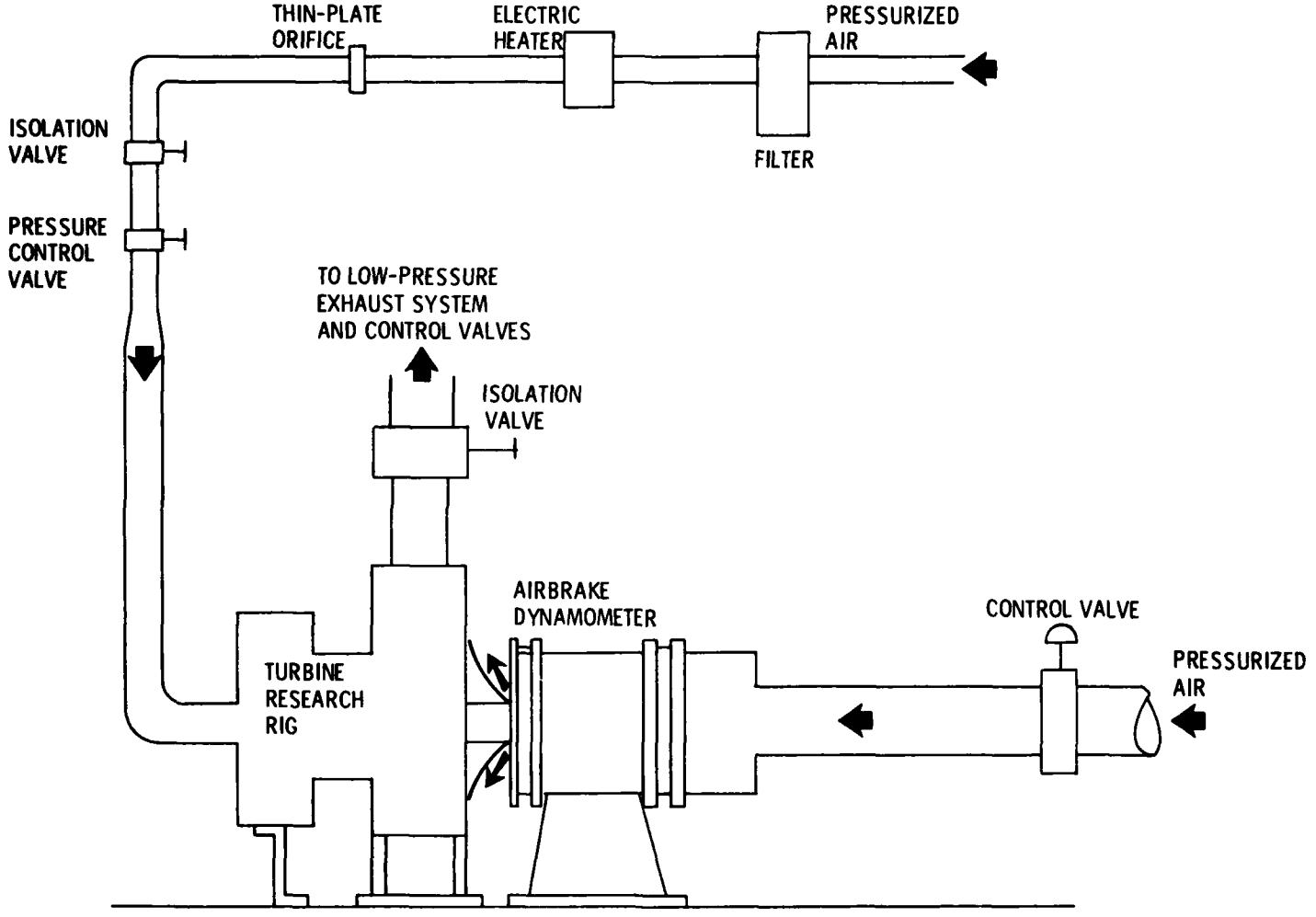

Figure 2. - Schematic of piping and test equipment.

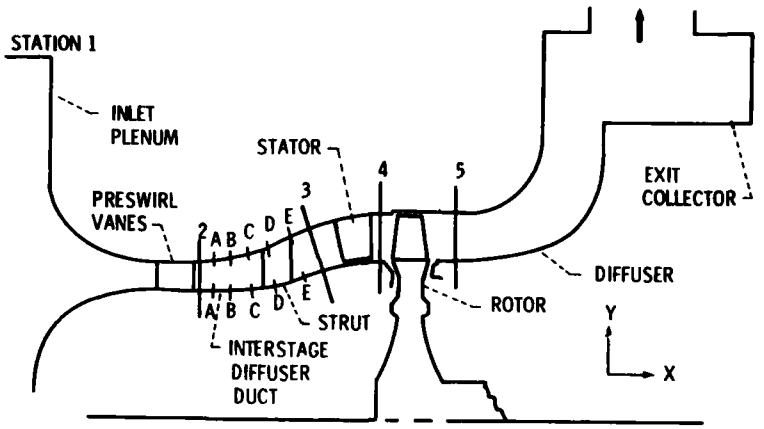

(a) Turbine flowpath and measuring stations.

Figure 3. - Research turbine flowpath and instrumentation.

◇ WALL STATIC PRESSURE TAPS
□ SURVEY PROBE: FLOW ANGLE, TOTAL PRESSURE, AND TOTAL TEMPERATURE
○ THERMOCOUPLE RAKE

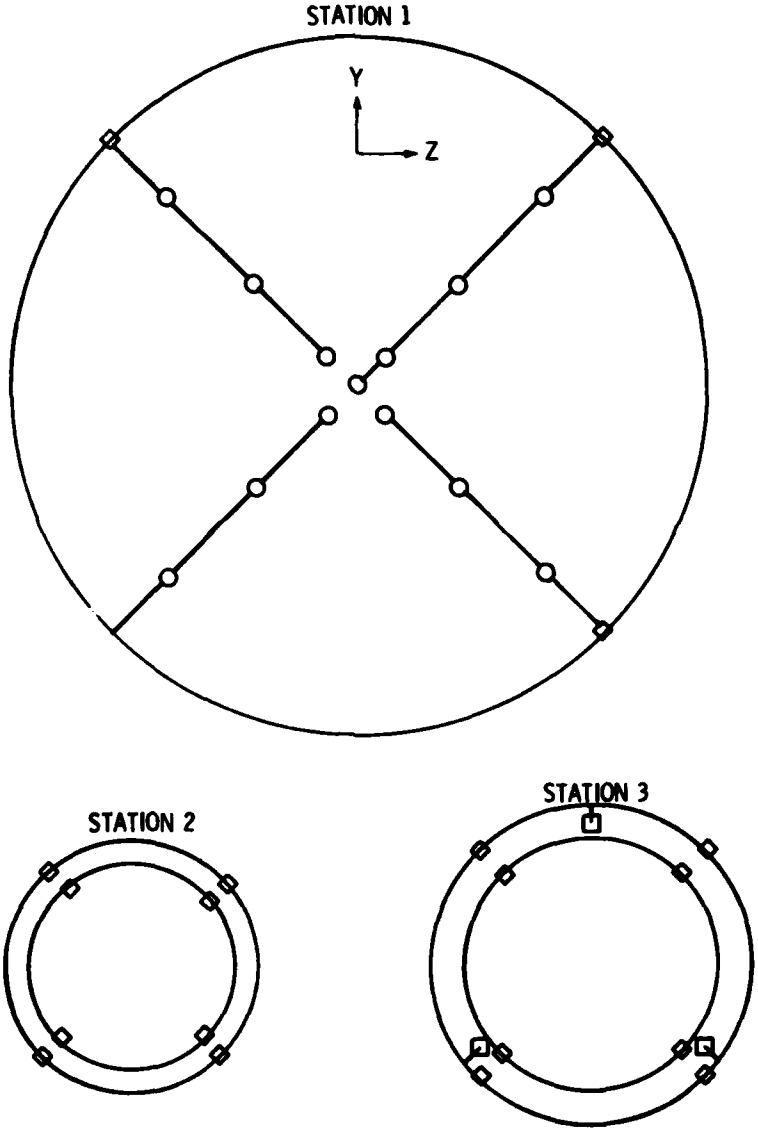

(b) Research instrumentation.

Figure 3. - Continued.

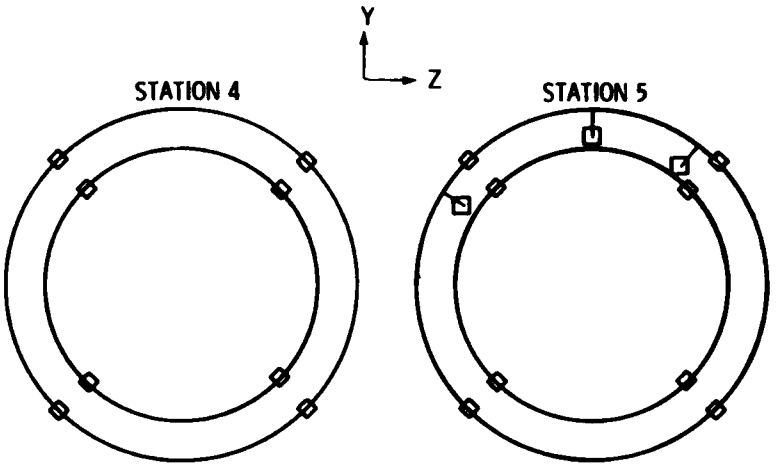

(b) Research instrumentation (continued).

Figure 3. - Concluded.

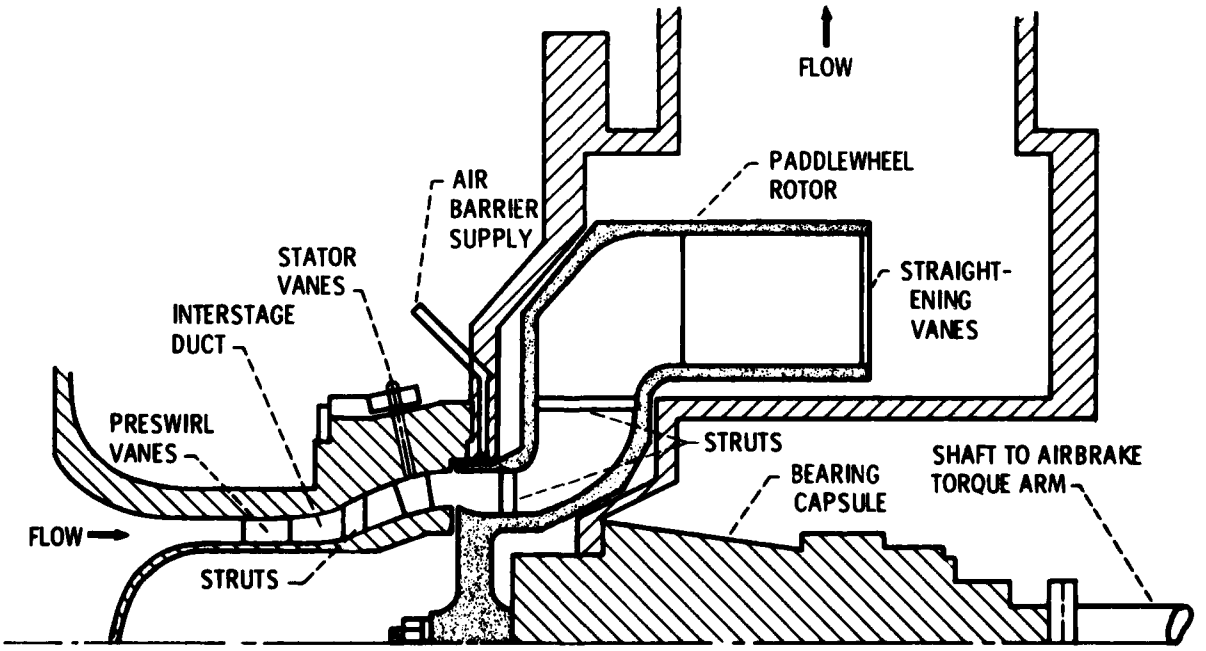

Figure 4. - Schematic of paddlewheel setup for stator performance tests.

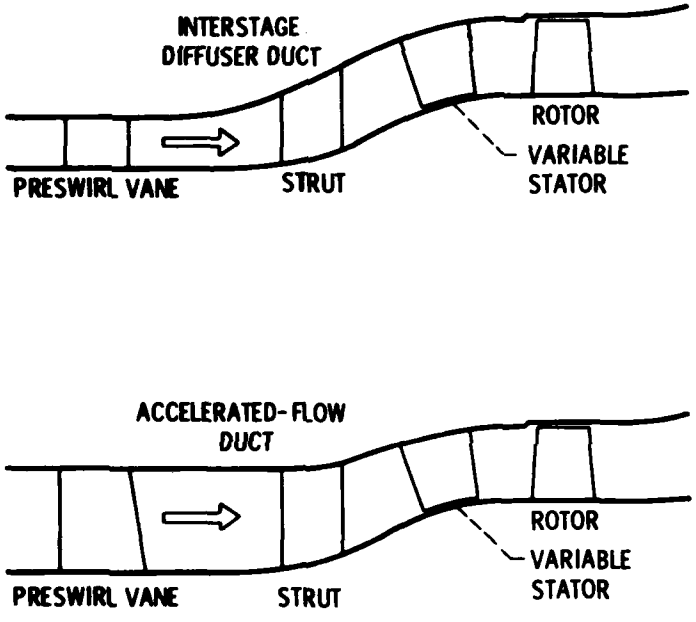

Figure 5. - Comparison of meridional flow path for the interstage diffuser duct and the accelerated-flow duct.

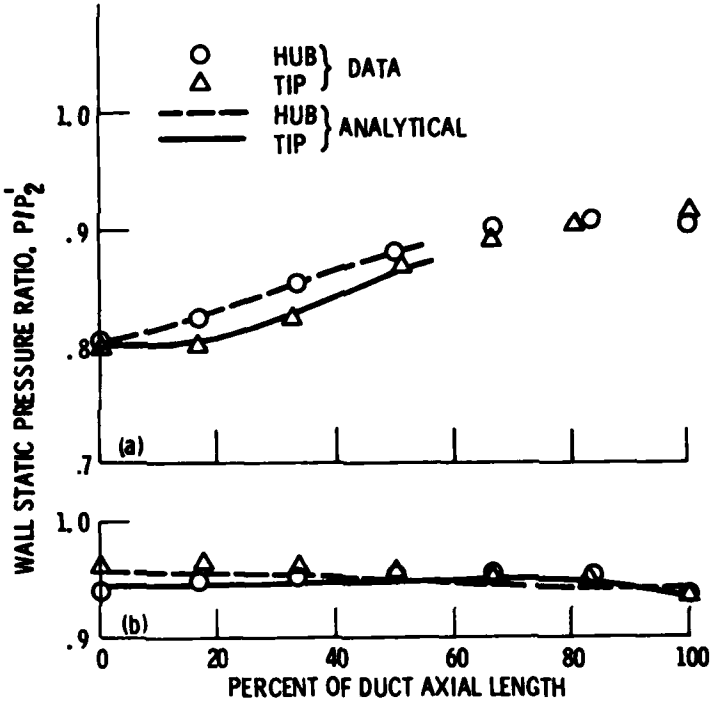

(a) Interstage diffuser duct.

(b) Accelerated flow inlet duct.

Figure 6. - Variations of wall static pressure through turbine inlet ducts based on measured data and analytical results near design mass flow rate.

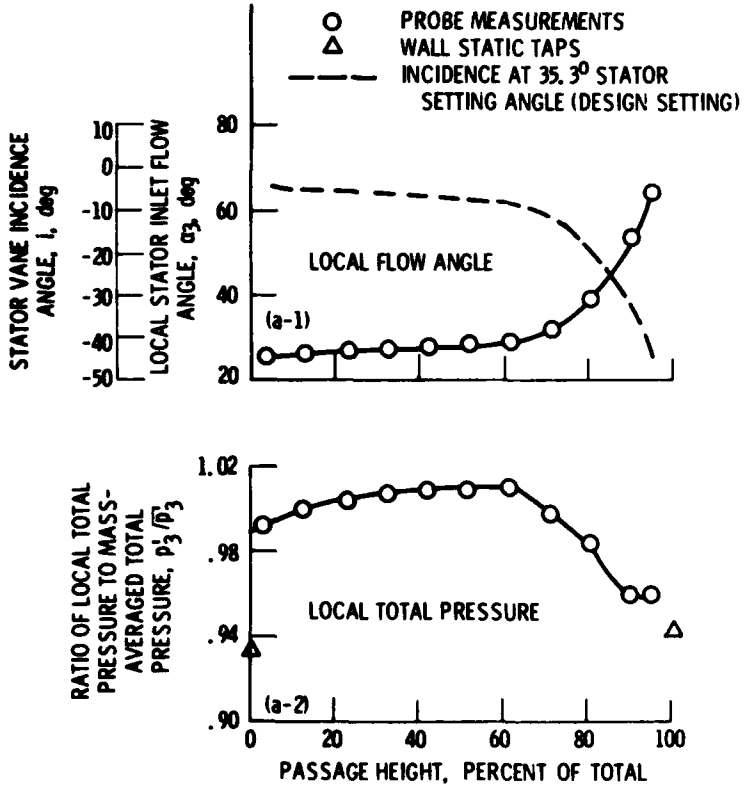

(a) Equivalent mass flow rate, 0.5654 kg/s.

Figure 7. - Radial variation of stator inlet flow angle, incidence angle, and total pressure for interstage diffuser duct.

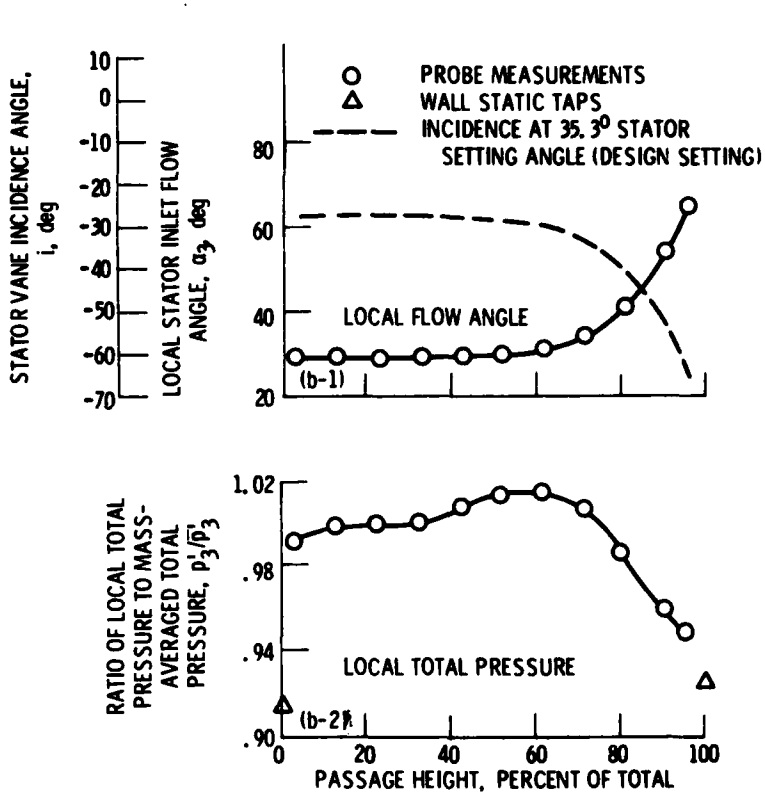

(b) Equivalent mass flow rate, 0.6417 kg/s.

Figure 7. - Continued.

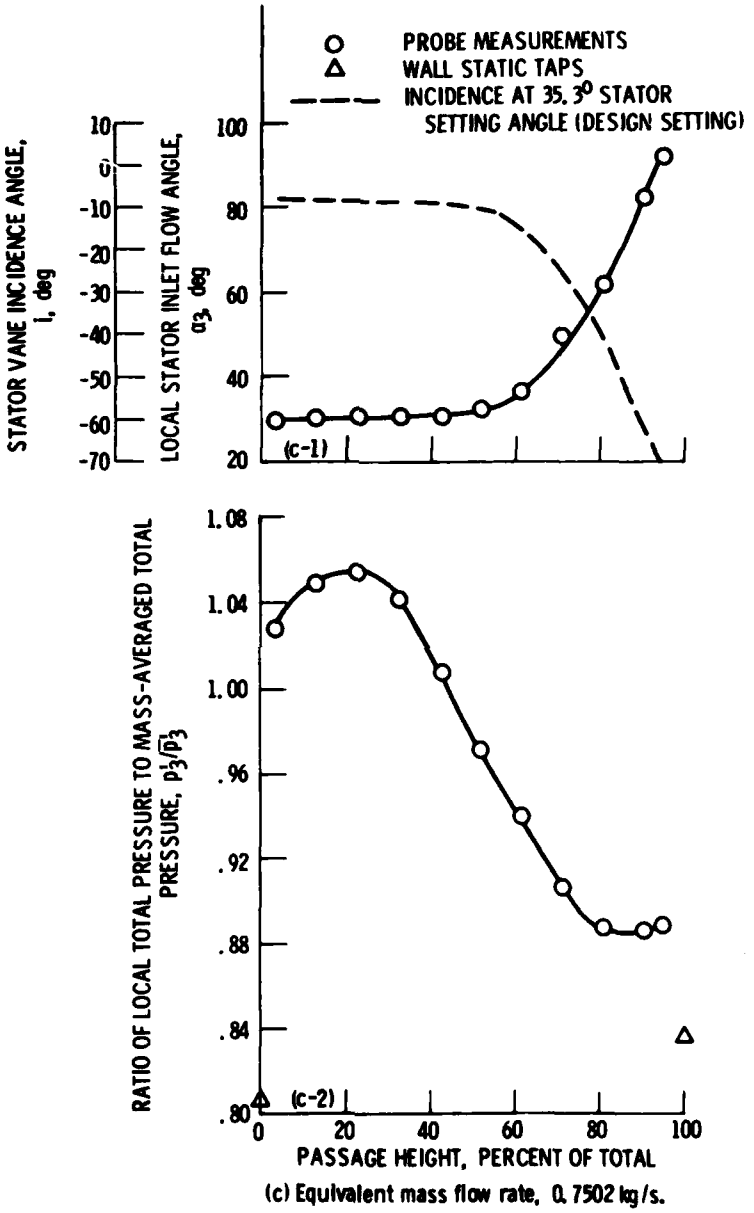

(c) Equivalent mass flow rate, 0.7502 kg/s.

Figure 7. - Concluded.

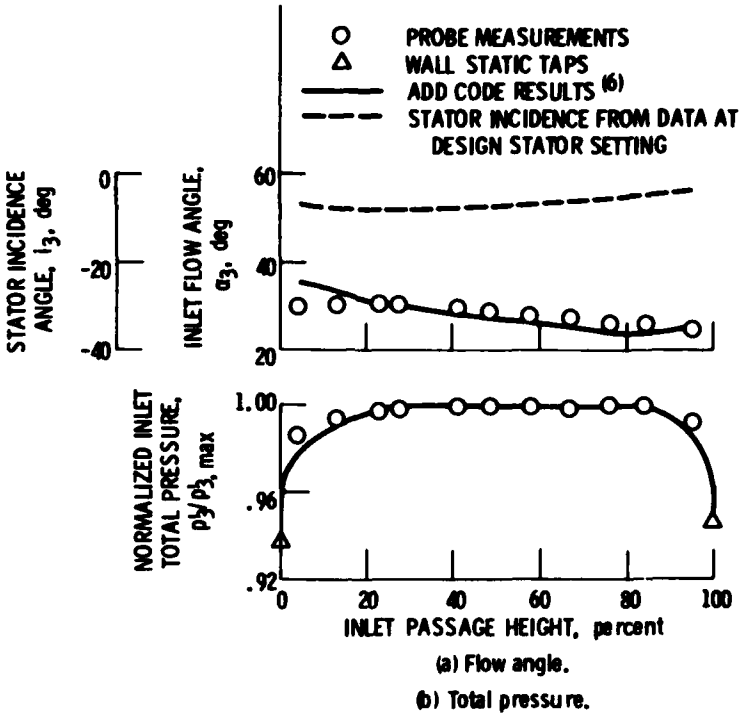

(a) Flow angle.

(b) Total pressure.

Figure 8. - Radial variation of stator inlet flow angle, incidence angle and total pressure for accelerated flow duct at equivalent mass flow rate of 0.620 Kg/s.

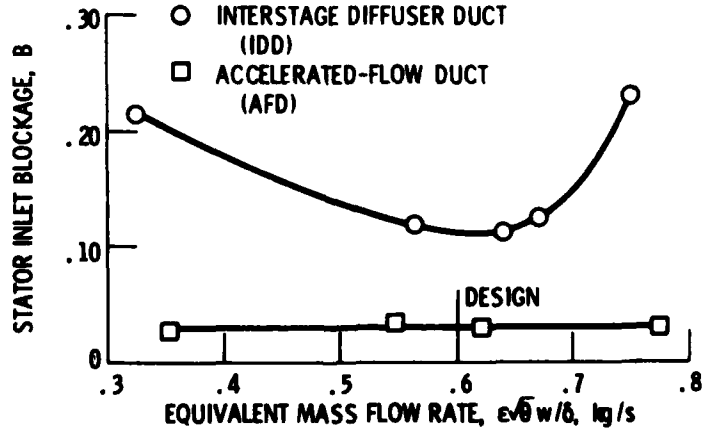

Figure 9. - Comparison of stator inlet flow blockage for interstage diffuser and accelerated-flow ducts from survey data over the range of mass flow rate tested.

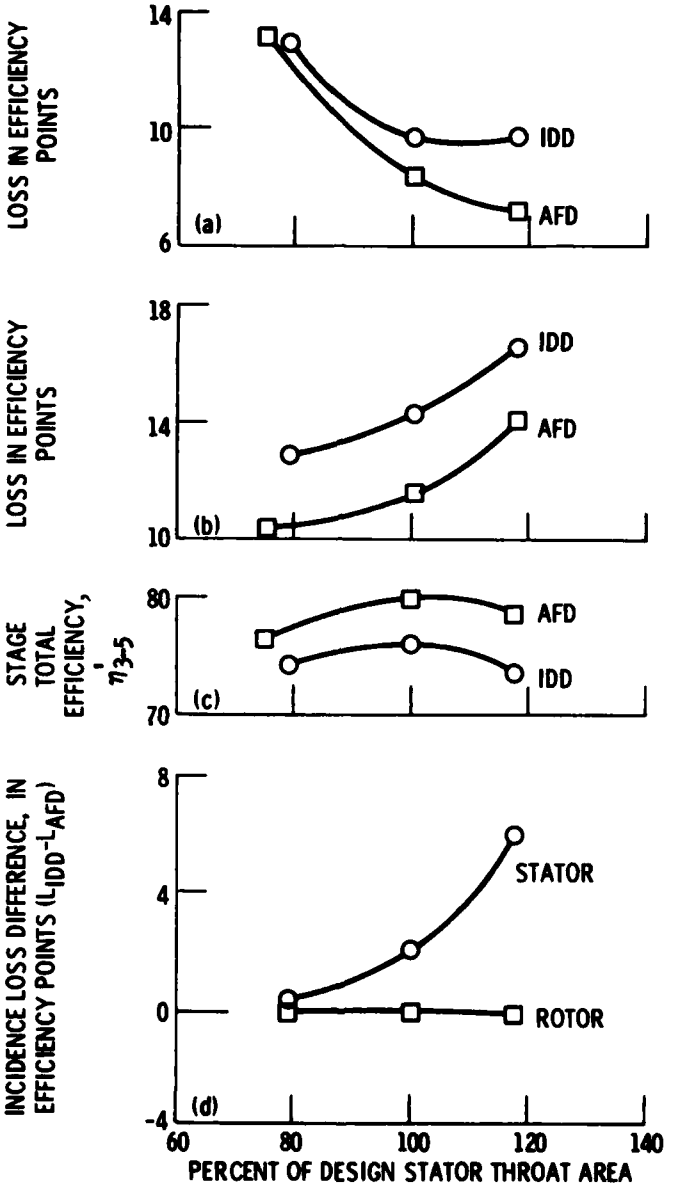

(a) Stator.

(b) Rotor.

(c) Stage.

(d) Incidence loss.

Figure 10. - Turbine component losses at design speed and work.

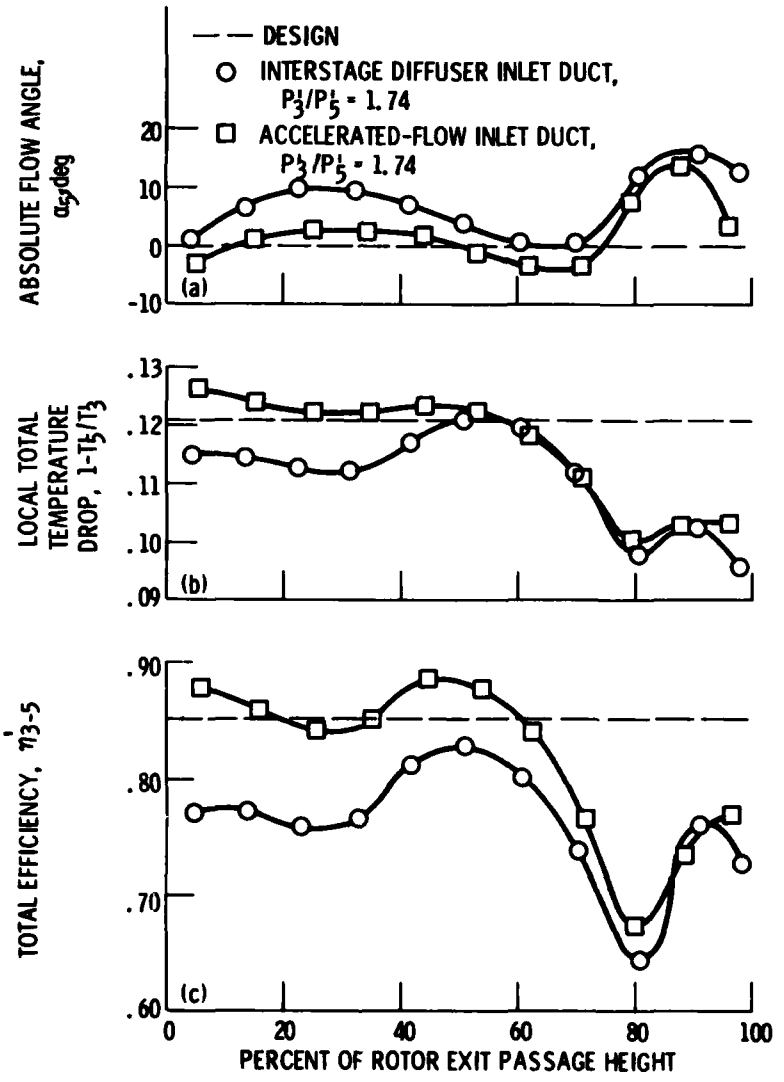

(a) Rotor exit absolute flow angle.

(b) Total temperature drop.

(c) Turbine blading total efficiency.

Figure 11. - Comparison of rotor exit survey results for interstage diffuser and accelerated-flow ducts at equivalent design speed and design stator throat area.

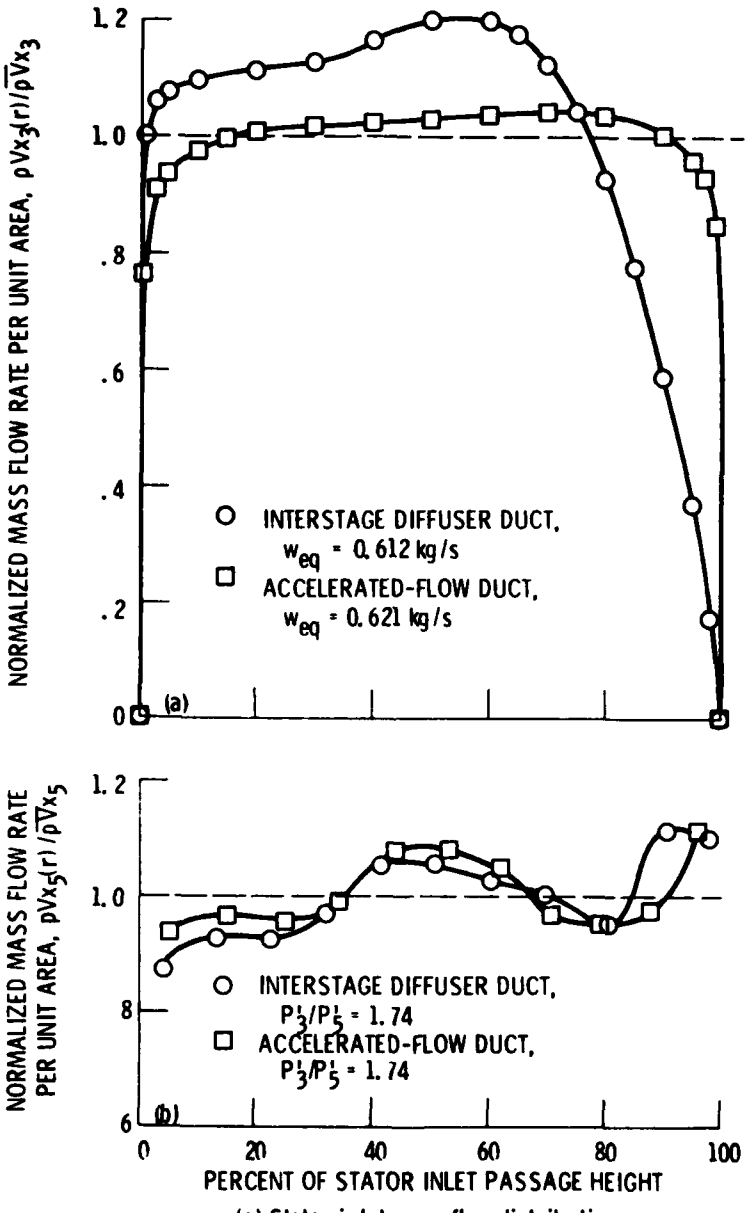

(a) Stator inlet mass flow distribution.

(b) Rotor exit mass flow distribution.

Figure 12. - Variation of normalized mass flow rate per unit area across passage at stator inlet and rotor exit.

1. Report No. NASA TM-83359 AVRADCOM-TR-83-C-2; AIAA-83-1179	2. Government Accession No	3. Recipient's Catalog No
4. Title and Subtitle EFFECTS OF INTERSTAGE DIFFUSER FLOW DISTORTION ON THE PERFORMANCE OF A 15.41-CENTIMETER TIP DIAMETER AXIAL POWER TURBINE		5. Report Date 6. Performing Organization Code
7. Author(s) Kerry L. McLallin, Milton G. Kofskey and Kestutis C. Civinskas		8. Performing Organization Report No E-1621 10. Work Unit No
9. Performing Organization Name and Address National Aeronautics and Space Administration Lewis Research Center and AVRADCOM Research and Technology Laboratories Cleveland, Ohio 44135		11. Contract or Grant No 13. Type of Report and Period Covered Technical Memorandum
12. Sponsoring Agency Name and Address U.S. Department of Energy Office of Vehicle and Engine R&D Washington, D.C. 20545		14. Sponsoring Agency Code DOE/NASA/51040-46

15. Supplementary Notes

Final report. Prepared under Interagency Agreement DE-AI01-77CS51040. Kerry L. McLallin and Milton G. Kofskey, NASA Lewis Research Center; Kestutis C. Civinskas, Propulsion Laboratory, AVRADCOM Research and Technology Laboratories, Lewis Research Center.

16. Abstract

The performance of a variable-area stator, axial flow power turbine was determined in a cold-air component research rig for two inlet duct configurations. The two ducts were an interstage diffuser duct and an accelerated-flow inlet duct which produced stator inlet boundary layer flow blockages of 11 percent and 3 percent, respectively. Turbine blade total efficiency at design point was measured to be 5.3 percent greater with the accelerated-flow inlet duct installed due to the reduction in inlet blockage. Blade component measurements show that of this performance improvement, 35 percent occurred in the stator and 65 percent occurred in the rotor. Analysis of inlet duct internal flow using an Axisymmetric Diffuser Duct Code (ADD Code) were in substantial agreement with the test data.

17. Key Words (Suggested by Author(s))	18. Distribution Statement		
Variable-area; Axial-flow turbine; Flow Flow distortion; Experimental performance	Unclassified - unlimited STAR Category 07 DOE Category UC-90		
19. Security Classif. (of this report) Unclassified	20. Security Classif. (of this page) Unclassified	21. No. of Pages	22. Price* A02

* For sale by the National Technical Information Service, Springfield, Virginia 22161

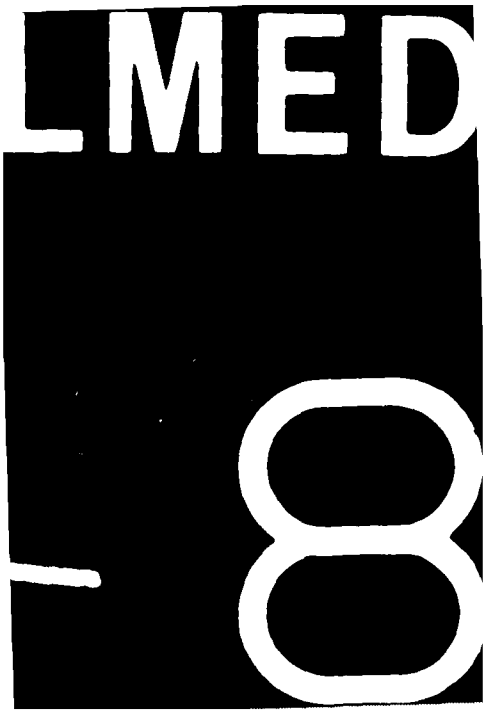
LMED
8